Journal of Membrane Science 658 (2022) 120761

Contents lists available at ScienceDirect

Journal of Membrane Science

journal homepage: www.elsevier.com/locate/memsci

Dual-layered covalent organic framework/MXene membranes with short paths for fast water treatment

Chao Feng [a], Kaiqin Ou [a], Zhipeng Zhang [b], Yongpeng Liu [a], Yunpeng Huang [a], Zicheng Wang [a], Yan Lv [a], Yue-E Miao [c], Yong Wang [b], Qianqian Lan [a,*], Tianxi Liu [a,**]

[a] The Key Laboratory of Synthetic and Biological Colloids, Ministry of Education, School of Chemical and Material Engineering, International Joint Research Laboratory for Nano Energy Composites, Jiangnan University, Wuxi, 214122, Jiangsu, PR China
[b] State Key Laboratory of Materials-Oriented Chemical Engineering, College of Chemical Engineering, Nanjing Tech University, Nanjing, 211816, Jiangsu, PR China
[c] State Key Laboratory for Modification of Chemical Fibers and Polymer Materials, College of Materials Science and Engineering, Innovation Center for Textile Science and Technology, Donghua University, Shanghai, 201620, PR China

ARTICLE INFO

Keywords:
MXene
Covalent organic framework
Ultrathin membrane
High flux
Water treatment

ABSTRACT

MXenes are receiving growing attention in wastewater treatment, but the preparation of ultrathin MXene membranes with short water pathways on macroporous substrates for improving flux is challenging due to the deformation of the flexible MXene nanosheets. Herein, we demonstrate the fabrication of ultrathin MXene membranes by constructing an intermediate porous covalent organic framework (COF) layer. COF nanosheets are first vacuum filtrated on macroporous substrates to form a porous COF layer, followed by the vacuum deposition of MXene nanosheets to produce the dual-layered COF/MXene composite membranes. The COF layer provides a smooth surface with rich pores and good hydrophilicity for depositing MXene nanosheets, leading to the well-assembled MXene layer as thin as 8 nm. The ultrathin MXene layer and the porous COF layer enable the short water transport pathways, and the well-assembled MXene nanosheets guarantee the narrow interlayer nanochannels. Membranes thereby are endowed with high permeance of 563 L/(m^2·h·bar) and high rejection to congo red of 99.6%, outperforming other reported COF- or MXene-based membranes. This work suggests a facile construction strategy of ultrathin MXene-based composite membranes with high separation performances, which are highly desired in water treatment.

1. Introduction

The shortage of water resource worldwide aggravated by increasing population and environmental pollution appeals for the efficient water purification technologies to produce clean water [1–3]. Membrane separation technologies have proven viable in water purification with decades of productive use because of their distinct advantages, including high water quality, excellent separation efficiency, low energy-consumption, and easy maintenance [4,5]. To design state-of-the-art separation membranes with high fluxes and efficient solute rejections, ultrathin thicknesses and uniform pore structures are always actively pursued [6–10]. Although various methods and materials have been proposed to develop membranes with higher separation performances [11,12], further improvement is hindered by the well-known trade-off effect between flux and rejection [13–15]. Therefore, advanced membranes with both high fluxes and high rejections are highly desired but still need to be explored.

Due to the atomic thickness, micrometer lateral size, and good solution processability, two-dimensional (2D) nanomaterials have shown great potential in constructing ultrathin membranes with narrow interlayer nanochannels to deliver exceptional separation performances [16–18]. As a young and important type of 2D nanomaterials, the carbides and/or nitrides of transition metals (MXenes) exemplified by $Ti_3C_2T_x$ are featured with rich surface chemistry, large specific surface area, high conductivity, and good mechanical strength [19–21]. Because of the evenly distributed groups (T_x: –O, –OH and/or –F) on entire surface of MXene nanosheets, the stacked MXene nanosheets exhibit more uniform and well-aligned nanochannels than other 2D nanomaterials [22–24]. However, the transport pathways through the interlayer nanochannels are long and tortuous, which hinders the mass

* Corresponding author.
** Corresponding author.
E-mail addresses: lanqianqian@jiangnan.edu.cn (Q. Lan), txliu@jiangnan.edu.cn (T. Liu).

https://doi.org/10.1016/j.memsci.2022.120761
Received 20 May 2022; Received in revised form 18 June 2022; Accepted 19 June 2022
Available online 22 June 2022

transfer and declines the water permeation through the MXene membranes [25]. According to the Hagen-Poiseuille equation, $P = \pi \cdot (R^4 \cdot \Delta p)/(8 \cdot \eta \cdot L)$, higher water permeance (P) can be achieved by increasing the diameter (R) and decreasing the length (L) of the transport pathways [26]. Variety of intercalators have been introduced into MXene membranes for enlarging interlayer nanochannels, but expected water permeance is hardly available due to the steric effect of the intercalators and the selectivity is inevitably declined in most cases [27–29]. For shortening the length of the transport pathways, designing thinner membranes with less tortuous pathways is the evident approach. To this end, intrinsically porous 2D nanosheets such as covalent organic frameworks (COFs) are recently popular as the nanofillers for providing shorter and more straightforward pathways [30–32]. Unfortunately, porous 2D nanosheets are randomly distributed in the hybrid membranes. As a result, the hybrid membranes with ultrathin thicknesses would suffer from low rejections due to the free penetration of solutes across the membranes through the porous 2D nanosheets [33]. Therefore, developing ultrathin and well-assembled MXene-based membranes with short pathways for fast water permeation and selective solute rejection is highly demanded but challenging.

Previous studies have revealed that the surface properties of the substrates including roughness and pore size can significantly influence the formation of laminates during the vacuum-derived membrane fabrication process [34,35]. Ultrathin nanosheet laminates deposited on macroporous substrates are of inferior stability and integrity because the flexible nanosheets cannot tolerate the deformation and maintain self-supporting. Consequently, well-assembled MXene membranes with the thicknesses down to tens of nanometers are hard to be realized [36]. Recently, building an intermediate scaffold layer to adjust the roughnesses and pore sizes of the substrates has been reported as an effective strategy to prepare thin film composite membranes with ultrathin thicknesses and improved performances [37,38]. Therefore, we expect that the scaffold-deposited substrates would also enable the formation of MXene membranes with unprecedentedly ultrathin thicknesses for enhancing fluxes and maintaining high rejections.

Herein, we prepare the dual-layered COF/MXene composite membranes by constructing an intermediate COF layer on macroporous substrates followed by the deposition of MXene nanosheets (Fig. 1). The COF layer possesses rich pores and is smoother and more hydrophilic than the substrate, facilitating the formation of the well-assembled MXene layer with the thickness down to 8 nm. Such a dual-layered composite structure offers short water transport pathways, endowing the membranes with superior separation performances exceeding other membranes reported in literature.

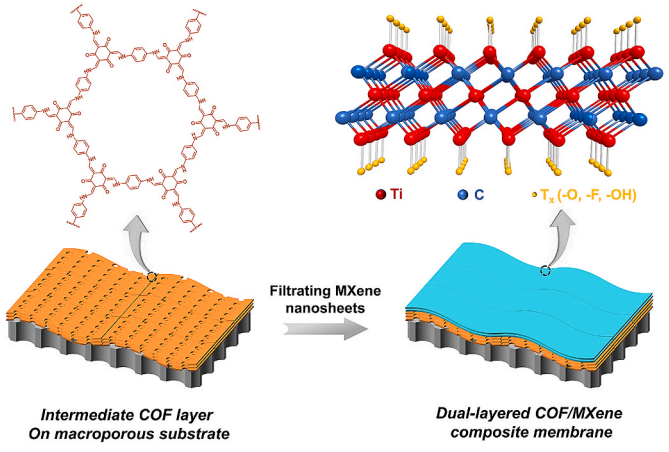

Fig. 1. Schematic illustration for the preparation of the dual-layered COF/MXene composite membranes.

2. Experimental section

2.1. Materials

Macroporous Nylon membranes with the nominal pore size of 0.2 μm and the diameter of 4.7 cm, macroporous polyethersulfone (PES) and mixed cellulose ester (MCE) membranes with the nominal pore size of 0.2 μm and the diameter of 5.0 cm were purchased from Jinteng Experimental Equipment Co. Ltd. MAX (Ti_3AlC_2) powder (200 mesh) was supplied by 11 Technology Co. Ltd. Lithium fluoride (LiF, 99.9%) and p-phenylenediamine (Pa, 99%) were provided by Aladdin. 1,3,5-triformylphloroglucinol (Tp, 98%) was bought from Yanshen Technology Co. Ltd. Hydrochloric acid (HCl, 36%), acetic acid (99.5%), glycerol (99%), ethanol (99.7%), and sodium hydroxide (NaOH, 96%) were provided by Sinopharm Chemical Reagent Co. Ltd. Evans blue, congo red, acid fuchsin, rhodamine B, and methyl orange were purchased from Innochem Co. Ltd. All chemicals were used as received. Deionized water (Millipore) was used in all the experiments.

2.2. Synthesis of COF nanosheets

12.6 mg of Tp and 9.6 mg of Pa were separately dissolved in 30 mL of glycerol under stirring at room temperature for 10 h and then mixed, followed by adding 1 mL of acetic acid. After further stirring at room temperature for 2 h, the mixture was transferred to a Shrek tube for pumping to remove the air. After heating at 120 °C for 72 h, the COF nanosheet dispersion with the concentration of 0.36 mg/mL was obtained.

2.3. Synthesis of MXene nanosheets

$Ti_3C_2T_x$ MXene nanosheets were prepared via a mild in situ hydrogen fluoride (HF) method reported in literature [39]. Briefly, 2 g of LiF were first dissolved in 30 mL of 6 mol/L HCl solution, followed by the addition of 2 g of Ti_3AlC_2. After stirring at 35 °C for 24 h, the precipitates were centrifugally collected and washed with water for several times until the pH value of the supernatant reached neutral. Afterwards, the slurry was redispersed in water by ultrasonication in an ice bath for 1 h under flowing nitrogen to delaminate MXene nanosheets. The unexfoliated bulks were then removed by centrifugation at 3500 rpm for 40 min, and the MXene nanosheet dispersion with the concentration of 1.8 mg/mL was obtained.

2.4. Preparation of dual-layered COF/MXene composite membranes

The dual-layered COF/MXene composite membranes were prepared by a vacuum filtration method using macroporous Nylon membranes as the substrates. Nylon membranes were first modified by immersing in 1 mol/L NaOH aqueous solution at 60 °C for 3 h. The COF nanosheet dispersion and the MXene nanosheet dispersion were diluted with ethanol to the concentration of 0.01 mg/mL and 0.025 mg/mL, respectively. To prepare the dual-layered COF/MXene composite membranes, different volumes of the diluted COF nanosheet dispersion and MXene nanosheet dispersion were vacuum filtrated onto the Nylon membranes in sequence, followed by vacuum drying at room temperature for 12 h. Membranes before and after depositing MXene nanosheets are named as COF_x membrane and $COF_x/MXene_y$ membrane, where x and y represent the masses (μg) of the deposited COF and MXene nanosheets, respectively.

2.5. Characterizations

Scanning electron microscopy (SEM) images were obtained on a Hitachi S-4800 microscope operated at the voltage of 5 kV and the current of 10 μA. The lateral sizes of nanosheets and the thicknesses of membranes were measured using the software Nano Measurer based on

the corresponding SEM images. Elemental distribution on the samples was scanned by energy-dispersive X-ray spectroscopy (EDS) with a Hitachi S-4800 at 30 kV. Transmission electron microscopy (TEM) images were obtained on a Hitachi JEM-2100 plus microscope. Atomic force microscopy (AFM) images were obtained on a Bruker MULTIMODE 8 instrument in the tapping mode at room temperature. X-ray diffraction (XRD) analysis was performed using a Bruker D2 PHASER spectrometer. Fourier transform infrared spectroscopy (FTIR) spectra were obtained on a Nicolet iS50 spectrometer at the attenuated total reflection mode. Water contact angles were measured using a Delphi OCA15EC video optical contact angle measuring instrument.

2.6. Evaluation of separation properties

The water permeances and rejection rates of the membranes were examined using a dead-end filtration device (Jiuling Technology) under the pressure of 0.3 bar. The effective membrane area for water permeation is 10.18 cm^2. The pure water permeance (*PWP*, L/(m^2·h·bar)) was calculated according to equation (1):

$$PWP = V/(A \cdot \Delta t \cdot P) \quad (1)$$

where V (L) is the water volume pass through the membrane, A (m^2) is the effective membrane area for water permeation, Δt (h) is the operation time, and P (bar) is the test pressure. To determine the rejection rates of the membranes, dyes dissolved in water at the concentration of 0.1 g/L were used as the feed solutions. Concentrations of the feed and the permeation solutions were measured using a UV–vis absorption spectrometer (Shimadzu UV-3600 plus). The rejection rate (R, %) was calculated according to equation (2):

$$R = (1\text{-}C_P/C_F) \times 100\% \quad (2)$$

where C_P and C_F (g/L) are the concentrations of the permeation and the feed solutions, respectively.

3. Results and discussion

3.1. Preparation of MXene and COF nanosheets

The $Ti_3C_2T_x$ MXene nanosheets were prepared via a mild in situ HF method. The morphologies of the Ti_3AlC_2 powder and the $Ti_3C_2T_x$ MXene nanosheets were first investigated. The parent Ti_3AlC_2 powder is in the plate-like morphology (Fig. 2a). After selectively etching the Al layers, the obtained dispersion of the MXene nanosheets exhibits the colloidal Tyndall effect (Fig. 2b). As shown in Fig. 2c, the lateral sizes of the MXene nanosheets are 0.6–3 μm. The TEM image in Fig. 2d depicts the ultrathin and uniform structures of the MXene nanosheets. The thickness of the MXene nanosheets determined by AFM is ~1.7 nm (Fig. 2e). We then performed XRD analysis to evaluate the exfoliation of the MXene nanosheets. As shown in Fig. 2f, the 104 peak at ~38.8° and the 002 peak at ~9.4° in the spectrum of the Ti_3AlC_2 powder are ascribed to the Al layers [40]. The 104 peak disappears in the spectrum of the $Ti_3C_2T_x$ MXene nanosheets and the 002 peak is shifted to ~5.5°, indicating the selective removal of the Al layers. Accordingly, the *d*-spacing of the $Ti_3C_2T_x$ MXene nanosheets is determined to be ~1.4 nm.

The COF nanosheets synthesized by a simple solvothermal reaction using Tp and Pa as the monomers were used in this work. The obtained COF nanosheets are well-dispersed in ethanol (Fig. 3a). Fig. 3b reveals that the obtained COFs are in the 2D sheet structures with the lateral sizes of 3–18 μm. The thickness of the COF nanosheets is uniform and determined to be ~4.2 nm (Fig. 3c and d). The synthesis of the COF nanosheets can be confirmed by FTIR analysis. As shown in Fig. 3e, Tp and Pa present the characteristic peaks of the stretching vibrations of C═O and N–H at ~1637 cm^{-1} and 3373-3188 cm^{-1}, respectively [41]. These peaks disappear in the spectrum of the TpPa COF nanosheets and new characteristic peaks of the stretching vibrations of C═C at ~1571 cm^{-1} and C–N at ~1251 cm^{-1} are observed, suggesting that Tp and Pa are completely transformed into TpPa with the β-ketoenamine structure [42]. Moreover, in the XRD pattern of the TpPa COF nanosheets, the 100 peak at ~4.7° and the 001 peak at ~27° indicate the intrinsic pore size of 1.8 nm and the *d*-spacing of 0.33 nm, respectively (Fig. 3f). These results demonstrate the successful synthesis of the TpPa COF nanosheets [43].

3.2. Fabrication of dual-layered COF/MXene composite membranes

The dual-layered COF/MXene composite membranes were fabricated by vacuum filtrating the MXene nanosheets on the COF nanosheet-deposited Nylon substrates. As shown in Fig. S1, the Nylon substrate pretreated with NaOH is white whereas the COF membrane is orange, suggesting that the COF nanosheets are uniformly deposited on the surface of the substrate. By contrast, the COF nanosheets cannot be uniformly and completely deposited on the surface of the untreated Nylon substrate (Fig. S2) due to its rough surface [39]. After further depositing the MXene nanosheets, the membrane turns to be yellowish brown. As shown in Fig. S3, C, N, O, F, and Ti elements are homogeneously distributed on the surface of the $COF_{100}/MXene_{30}$ membrane, indicating the uniform deposition of COF and MXene nanosheets. We first investigated the morphologies of the membranes after depositing COF nanosheets. Fig. 4a shows the macropores with multi-distributed pore sizes ranging from hundreds of nanometers to a few micrometers on the surface of bare Nylon substrate. When 75 μg of the COF nanosheets are deposited on the substrate, the macropores and the skeletons

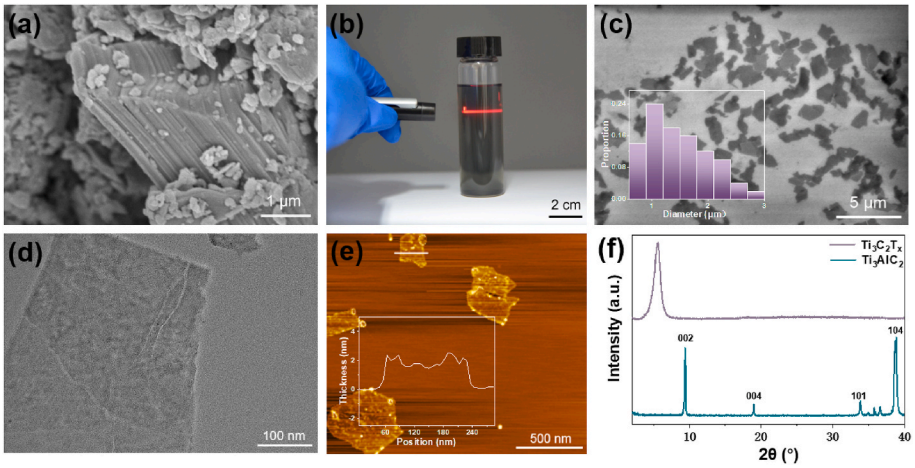

Fig. 2. Characterizations of the MXene nanosheets. (a) SEM image of the parent Ti_3AlC_2 powder. (b) Photograph of the dispersion of MXene nanosheets with the Tyndall effect. (c) SEM image of the MXene nanosheets dispersed on a silica wafer and the lateral size distribution of the MXene nanosheets. (d) TEM image of the MXene nanosheets. (e) AFM image and the corresponding height profile of the MXene nanosheets. (f) XRD patterns of the Ti_3AlC_2 powder and the $Ti_3C_2T_x$ MXene nanosheets.

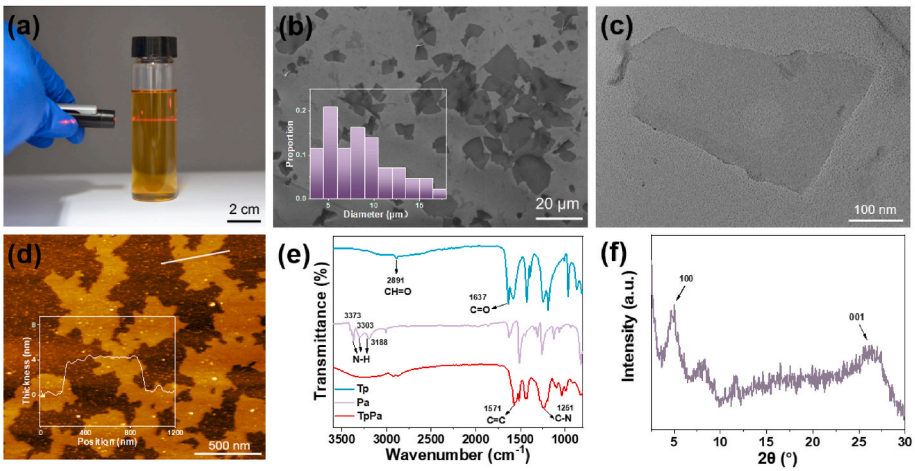

Fig. 3. Characterizations of the COF nanosheets. (a) Photograph of the dispersion of COF nanosheets with the Tyndall effect. (b) SEM image of the COF nanosheets dispersed on a silica wafer and the lateral size distribution of the COF nanosheets. (c) TEM image and (d) AFM image and the corresponding height profile of the COF nanosheets. (e) FTIR spectra of Tp, Pa, and TpPa COF nanosheets. (f) XRD pattern of the COF nanosheets.

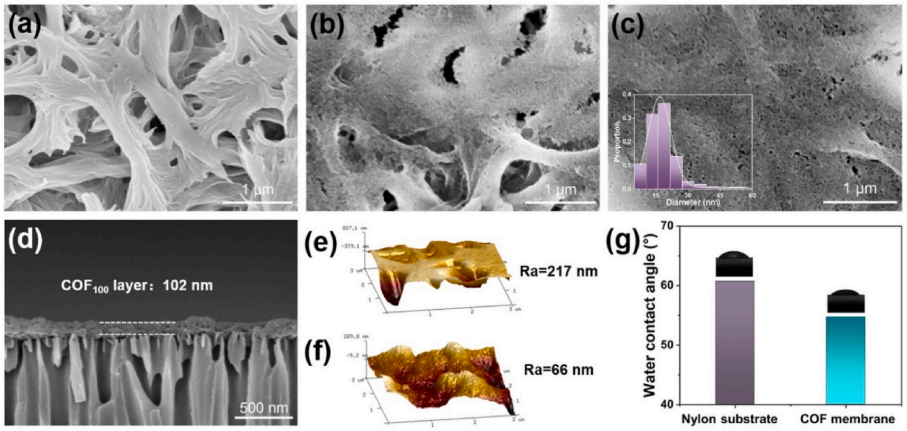

Fig. 4. Characterizations of the COF membranes. Surface SEM images of (a) the bare Nylon substrate pre-treated with NaOH, (b) the COF_{75} membrane, and (c) the COF_{100} membrane. Inset in (c) is the pore size distribution of the COF_{100} membrane. (d) Cross-sectional SEM image of the COF_{100} membrane. AFM surface topographies of (e) the bare Nylon substrate pre-treated with NaOH and (f) the COF_{100} membrane. (g) Water contact angles of the bare Nylon substrate pre-treated with NaOH and the COF_{100} membrane.

of the substrate remain visible (Fig. 4b). When the mass of the deposited COF nanosheets is increased to 100 μg, a continuously thin COF_{100} layer possessing rich and uniform pores with the average diameter of 16 nm is observed (Fig. 4c). These pores are formed due to the crispation of the defective regions between small COF crystallites [44,45]. which are abbreviated as crispation-induced pores and are generated during the drying process (Fig. S4). To clearly examine the cross-sectional morphologies of the membranes, we prepared the membranes on porous alumina (AAO) substrates with other conditions unchanged. As shown in Fig. 4d, the thickness of the COF_{100} layer is ~102 nm. Further increasing

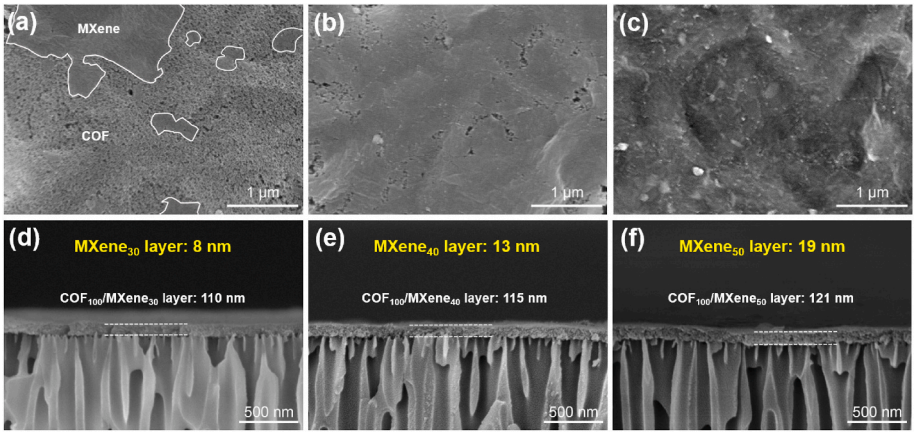

Fig. 5. Morphologies of the dual-layered COF/MXene composite membranes. Surface SEM images of (a) the $COF_{100}/MXene_{10}$ membrane, (b) the $COF_{100}/MXene_{20}$ membrane, and (c) the $COF_{100}/MXene_{30}$ membrane. The MXene domains in (a) are highlighted with white curves. Cross-sectional SEM images of (d) the $COF_{100}/MXene_{30}$ membrane, (e) the $COF_{100}/MXene_{40}$ membrane, and (f) the $COF_{100}/MXene_{50}$ membrane.

the mass of the deposited COF nanosheets to 150 μg leads to a porous COF_{150} layer with higher thickness of ~165 nm (Fig. S5). We then characterized the surface roughnesses (Ra) of the bare substrate and the COF_{100} membrane, which are 217 nm and 66 nm, respectively (Fig. 4e and f). Moreover, the COF_{100} membrane exhibits stronger hydrophilicity than the bare substrate (Fig. 4g). These results indicate that the COF layer can modify the surface properties such as pore structure, roughness, and hydrophilicity of the bare substrate, which would facilitate the subsequent deposition of MXene nanosheets.

Afterwards, we deposited MXene nanosheets on the intermediate COF_{100} layers to fabricate the dual-layered COF/MXene composite membranes and investigated their morphologies. As shown in Fig. 5a, discrete and conformal MXene domains with sharp edges are observed after depositing 10 μg of the MXene nanosheets. With the increase in the mass of the deposited MXene nanosheets, the COF_{100} layer is gradually covered and exhibits less porous structures (Fig. 5b). When the mass of the deposited MXene nanosheets is further increased to 30 μg, 40 μg, and 50 μg, the obtained dual-layered COF/MXene composite membranes show dense and wrinkled surface morphologies, indicating the formation of the integrate MXene layers (Fig. 5c and Fig. S6). The interlayer space in the MXene layer is 0.3 nm thanks to the uniform deposition of MXene nanosheets on COF layer (Fig. S7). The thicknesses of the $COF_{100}/MXene_{30}$ layer, the $COF_{100}/MXene_{40}$ layer, and the $COF_{100}/MXene_{50}$ layer are ~110 nm, ~115 nm, and ~121 nm, respectively (Fig. 5d–f). Since the COF_{100} layer is in the thickness of ~102 nm as we discussed above, the thicknesses of the $MXene_{30}$ layer, the $MXene_{40}$ layer, and the $MXene_{50}$ layer are determined to be ~8 nm, ~13 nm, and ~19 nm, respectively. By contrast, when we directly deposited 130 μg of the MXene nanosheets on the bare substrate, the MXene layer shows lots of defects, suggesting the important role of the intermediate COF layer (Fig. S8). The smooth and hydrophilic COF layer covers the multi-distributed macropores of the substrate and provides extra pores including the intrinsic nanopores and the crispation-induced pores, leading to the uniform deposition and fine assembly of MXene nanosheets to form ultrathin and integrate MXene layer. The COF layer and the Nylon substrate are interacted with each other by non-covalent forces such as hydrogen-bonds and amphiphilic interactions, and the MXene layer and the COF layer are assembled together mainly by electrostatic interactions. Both the COF membrane and the dual-layered COF/MXene composite membrane maintain integrated without detachment after several folds, demonstrating the good stability of this three-layered composite structure (Fig. S9). Moreover, besides Nylon membranes, other types of macroporous membranes can also be used as the substrates. For example, in the presence of the intermediate COF layer, MXene nanosheets can be uniformly deposited on macroporous AAO membrane, PES membrane, and MCE membrane (Fig. S10), illustrating the generality of the intermediate COF layer approach.

3.3. Separation performances of dual-layered COF/MXene composite membranes

The dual-layered COF/MXene composite membranes are expected to achieve high separation performances thanks to the rich pores of the COF layers and the ultrathin thicknesses of the MXene layers. We first measured the water permeances and rejections to congo red of the COF membranes. As shown in Fig. 6a, the permeances of the COF_{75} membrane, the COF_{100} membrane, and the COF_{150} membrane are 4431 L/(m^2·h·bar), 3809 L/(m^2·h·bar), and 215 L/(m^2·h·bar), and their rejections are 25.7%, 47.2%, and 98.8%, respectively. The decreased permeances and increased rejections with the increase in the mass of the

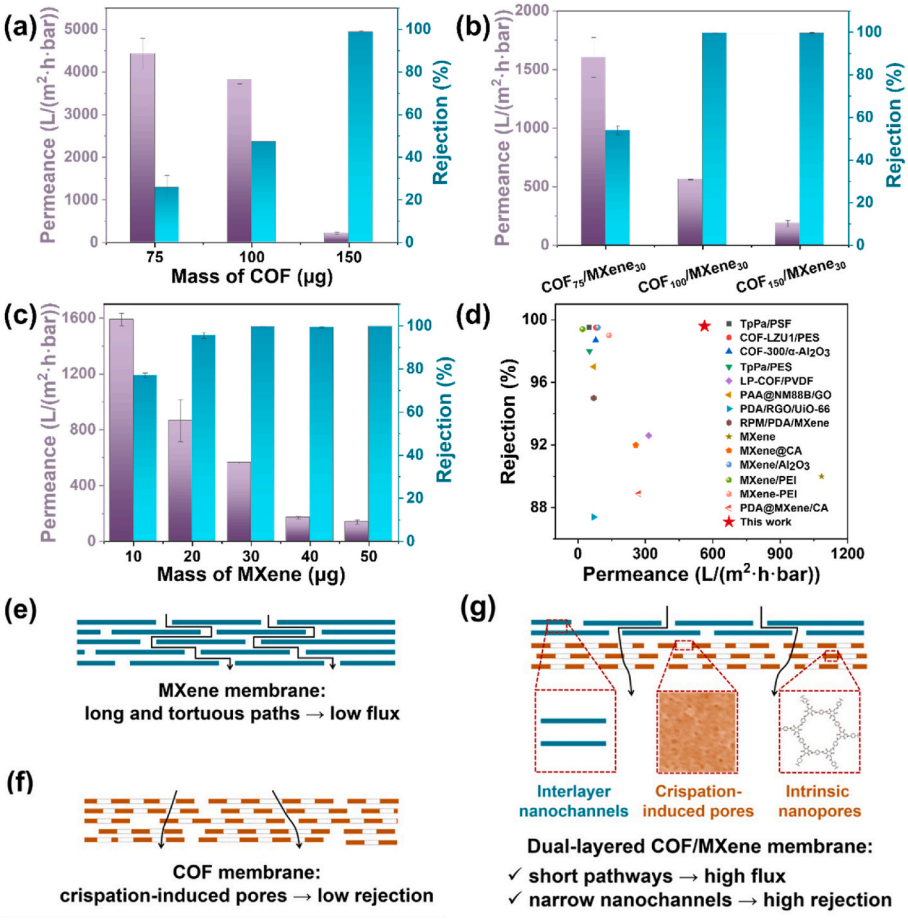

Fig. 6. Separation performances of the membranes. Water permeances and rejections of (a) the COF_{75}, COF_{100}, and COF_{150} membranes, (b) the $COF_{75}/MXene_{30}$, $COF_{100}/MXene_{30}$, and $COF_{150}/MXene_{30}$ membranes, and (c) the $COF_{100}/MXene_{10}$, $COF_{100}/MXene_{20}$, $COF_{100}/MXene_{30}$, $COF_{100}/MXene_{40}$, and $COF_{100}/MXene_{50}$ membranes. (d) Comparison of separation performances of the dual-layered COF/MXene composite membranes with other membranes. Schematic illustration for the structures of (e) pure MXene membrane, (f) pure COF membrane and (g) the dual-layered COF/MXene composite membrane.

COF nanosheets is due to the coverage of the macroporous substrates by the COF layers with increased thicknesses, the higher mass transfer resistances through the discrete crispation-induced pores inside the COF layers, and the constricted effective apertures derived by offset stacking of COF nanosheets. Moreover, when we deposited 30 μg of the MXene nanosheets on the above COF membranes, the COF_{75}/$MXene_{30}$ membrane exhibits a high permeance of 1602 L/(m^2·h·bar) but a low rejection of 53.9% (Fig. 6b). This is because the $MXene_{30}$ layer deposited on the defective COF_{75} membrane is unintegrated and allows both water and solutes to pass through the membrane (Fig. S11). The COF_{100} membrane can enable the formation of the defect-free $MXene_{30}$ layer as we discussed above, leading to the high rejection of 99.6% while remaining high permeance of 563 L/(m^2·h·bar) of the COF_{100}/$MXene_{30}$ membrane. In addition, the COF_{150}/$MXene_{30}$ membrane exhibits a low permeance of 187 L/(m^2·h·bar) ascribed to the thick COF_{150} layer. Therefore, the COF_{100} membrane is the optimal one for further preparation of the dual-layered COF/MXene composite membranes.

The separation performances of the dual-layered COF/MXene composite membranes fabricated by depositing MXene nanosheets with varied masses on the COF_{100} membranes were then examined. As shown in Fig. 6c, with the increase in the mass of the MXene nanosheets, the permeances of the dual-layered COF/MXene composite membranes are decreased while the rejections are increased. For example, the permeance of the COF_{100}/$MXene_{10}$ membrane is 1591 L/(m^2·h·bar), which is declined to 864 L/(m^2·h·bar) and 563 L/(m^2·h·bar) for the COF_{100}/$MXene_{20}$ membrane and COF_{100}/$MXene_{30}$ membrane, respectively. Meanwhile, their rejections are gradually increased from 77% to 95.6% and 99.6%, respectively. Further increasing the mass of the MXene nanosheets leads to severely declined permeances lower than 170 L/(m^2·h·bar). With the increase in the mass of the MXene nanosheets, the intermediate porous COF layers are gradually covered by the MXene layers with higher thicknesses, leading to the decreased permeances and the increased rejections. In addition, the rejections to dyes with different molecular weights of the COF_{100}/$MXene_{30}$ membrane were also evaluated (Fig. S12). The rejection rates are gradually increased with the increasing molecular weights of dyes, implying that the rejection of solutes is mainly dominated by the size-sieving effect. Accordingly, the molecular-weight-cut-off of the membrane is determined to be ~585.54 g/mol, which is defined as the molecular weight of solute at the rejection rate of 90%. Notably, the operation pressure should be controlled lower than 0.7 bar to avoid the structural compaction of the membranes (Fig. S13).

We compared the separation performances of the dual-layered COF/MXene composite membranes prepared in this work with other membranes reported in literature (Fig. 6d and Table S1). The dual-layered COF/MXene composite membrane shows 7–11 times higher permeance than other COF-based membranes with similar rejections [46, 47]. Meanwhile, compared with other MXene-based membranes [48, 49], the dual-layered COF/MXene composite membrane shows both higher permeance and rejection. As shown in Fig. 6e, pure MXene membrane prepared on macroporous substrate possesses high thickness to against deformation, resulting in long and tortuous pathways and thus low water fluxes. Porous COF membrane can provide short pathways for fast water permeation, but their large crispation-induced pores also allow the solutes to transport (Fig. 6f). By contrast, the construction of the intermediate COF layer can not only enable the formation of ultrathin and well-assembled MXene layer with narrow interlayer nanochannels, but also provide rich paths including the crispation-induced pores and the intrinsic nanopores for mass transport (Fig. 6g). Therefore, the high flux of the dual-layered COF/MXene composite membrane is contributed from the shortened pathways due to the ultrathin MXene layer and the porous COF layer, while the high rejection is enabled by the narrow interlayer nanochannels between the well-assembled MXene nanosheets.

4. Conclusions

In conclusion, we demonstrate the preparation of the dual-layered COF/MXene composite membranes with short pathways and narrow interlayer nanochannels for fast water treatment. The COF nanosheets are first deposited on macroporous substrate to form a smooth intermediate layer with rich pores, followed by vacuum filtrating the MXene nanosheets to generate an ultrathin MXene layer. Thanks to the well-deposited ultrathin MXene layer and the porous COF layer, the dual-layered COF/MXene composite membrane possesses narrow interlayer nanochannels and short water transport pathways, and exhibits superior separation performances than other COF- and MXene-based membranes reported in literature. This work demonstrates a facile method to prepare ultrathin MXene membranes, which is expected to be used in the preparation of other types of laminated membranes with enhanced performances.

Author statement

Chao Feng: Investigation, Formal analysis, Methodology, Writing – original draft, **Kaiqin Ou**: Investigation, Formal analysis, **Zhipeng Zhang**: Investigation, **Yongpeng Liu**: Investigation, **Yunpeng Huang**: Project administration, **Zicheng Wang**: Project administration, **Yan Lv**: Funding acquisition, **Yue-E Miao**: Supervision, **Yong Wang**: Supervision, **Qianqian Lan**: Supervision, Funding acquisition, Methodology, Writing – original draft, Writing – review & editing, **Tianxi Liu**: Supervision, Writing – review & editing.

Declaration of competing interest

The authors declare that they have no known competing financial interests or personal relationships that could have appeared to influence the work reported in this paper.

Data availability

Data will be made available on request.

Acknowledgment

Financial support from the National Natural Science Foundation of China (22008086, 22108030), the China Postdoctoral Science Foundation (2020M671332), and the Jiangsu Postdoctoral Science Foundation (2020Z210) is gratefully acknowledged.

Appendix A. Supplementary data

Supplementary data to this article can be found online at https://doi.org/10.1016/j.memsci.2022.120761.

References

[1] H. Zhang, Q. He, J. Luo, Y. Wan, S.B. Darling, Sharpening nanofiltration: strategies for enhanced membrane selectivity, ACS Appl. Mater. Interfaces 12 (36) (2020) 39948–39966, https://doi.org/10.1021/acsami.0c11136.
[2] W. Zhang, M. Yin, Q. Zhao, C. Jin, N. Wang, S. Ji, C.L. Ritt, M. Elimelech, Q. An, Graphene oxide membranes with stable porous structure for ultrafast water transport, Nat. Nanotechnol. 16 (3) (2021) 337–343, https://doi.org/10.1038/s41565-020-00833-9.
[3] X. Cheng, Y. Ye, Z. Li, X. Chen, Q. Bai, K. Wang, Y. Zhang, E. Drioli, J. Ma, Constructing environmental-friendly "oil-diode" janus membrane for oil/water separation, ACS Nano 16 (3) (2022) 4684–4692, https://doi.org/10.1021/acsnano.1c11388.
[4] J.R. Werber, C.O. Osuji, M. Elimelech, Materials for next-generation desalination and water purification membranes, Nat. Rev. Mater. 1 (5) (2016), 16018, https://doi.org/10.1038/natrevmats.2016.18.
[5] S. Ling, Z. Qin, W. Huang, S. Cao, D.L. Kaplan, M.J. Buehler, Design and function of biomimetic multilayer water purification membranes, Sci. Adv. 3 (4) (2017), e1601939, https://doi.org/10.1126/sciadv.1601939.

[6] Z. Zhou, Y. Hu, C. Boo, Z. Liu, J. Li, L. Deng, X. An, High-performance thin-film composite membrane with an ultrathin spray-coated carbon nanotube interlayer, Environ. Sci. Technol. Lett. 5 (5) (2018) 243–248, https://doi.org/10.1021/acs.estlett.8b00169.

[7] Z. Wang, R. Liu, Q. Lan, Y. Wang, Selective swelling blends of block copolymers for nanoporous membranes with enhanced permeability and robustness, J. Polym. Sci. B Polym. Phys. 55 (21) (2017) 1617–1625, https://doi.org/10.1002/polb.24419.

[8] Q. Lan, C. Feng, K. Ou, Z. Wang, Y. Wang, T. Liu, Phenolic membranes with tunable sub-10-nm pores for nanofiltration and tight-ultrafiltration, J. Membr. Sci. 640 (2021), 119858, https://doi.org/10.1016/j.memsci.2021.119858.

[9] Q. Lan, Z. Zhang, F. Xu, M. Wei, Y. Wang, Nanomeshes with sub-10 nm pores by glycerol-triggered 2D assembly in liquid phases for fast and selective membranes, Nano Lett. 21 (7) (2021) 3302–3309, https://doi.org/10.1021/acs.nanolett.1c00826.

[10] K. Celebi, J. Buchheim, R.M. Wyss, A. Droudian, P. Gasser, I. Shorubalko, J.-I. Kye, C. Lee, H.G. Park, Ultimate permeation across atomically thin porous graphene, Science 344 (6181) (2014) 289–292, https://doi.org/10.1126/science.1249097.

[11] M. Wu, F. Yang, J. Yang, Q. Zhong, V. Koerstgen, P. Yang, P. Mueller-Buschbaum, Z. Xu, Lysozyme membranes promoted by hydrophobic substrates for ultrafast and precise organic solvent nanofiltration, Nano Lett. 20 (12) (2020) 8760–8767, https://doi.org/10.1021/acs.nanolett.0c03632.

[12] K. Li, J. Zhu, D. Liu, Y. Zhang, B. Van der Bruggen, Controllable and rapid synthesis of conjugated microporous polymer membranes via interfacial polymerization for ultrafast molecular separation, Chem. Mater. 33 (17) (2021) 7047–7056, https://doi.org/10.1021/acs.chemmater.1c02143.

[13] L. Guo, Y. Wang, M. Steinhart, Porous block copolymer separation membranes for 21st century sanitation and hygiene, Chem. Soc. Rev. 50 (11) (2021) 6333–6348, https://doi.org/10.1039/d0cs00500b.

[14] Q. Lan, N. Yan, H. Yang, Y. Wang, Nanocomposite block copolymer membranes with enhanced permeance and robustness by carbon nanotube doping, Compos. Commun. 29 (2022), 101025, https://doi.org/10.1016/j.coco.2021.101025.

[15] A. Lee, J.W. Elam, S.B. Darling, Membrane materials for water purification: design, development, and application, Environ. Sci. Water Res. Technol. 2 (1) (2016) 17–42, https://doi.org/10.1039/c5ew00159e.

[16] Y. Kang, Y. Xia, H. Wang, X. Zhang, 2D laminar membranes for selective water and ion transport, Adv. Funct. Mater. 29 (29) (2019), 1902014, https://doi.org/10.1002/adfm.201902014.

[17] L. Ding, Y. Wei, L. Li, T. Zhang, H. Wang, J. Xue, L. Ding, S. Wang, J. Caro, Y. Gogotsi, MXene molecular sieving membranes for highly efficient gas separation, Nat. Commun. 9 (2018) 155, https://doi.org/10.1038/s41467-017-02529-6.

[18] Y. Zhang, D. Chen, N. Li, Q. Xu, H. Li, J. He, J. Lu, High-performance and stable two-dimensional MXene-polyethyleneimine composite lamellar membranes for molecular separation, ACS Appl. Mater. Interfaces 14 (8) (2022) 10237–10245, https://doi.org/10.1021/acsami.1c20540.

[19] H.E. Karahan, K. Goh, C. Zhang, E. Yang, C. Yıldırım, C.Y. Chuah, M.G. Ahunbay, J. Lee, Ş.B. Tantekin-Ersolmaz, Y. Chen, T.-H. Bae, MXene materials for designing advanced separation membranes, Adv. Mater. 32 (29) (2020), 1906697, https://doi.org/10.1002/adma.201906697.

[20] J. Shen, J. Yuan, B. Shi, X. You, R. Ding, T. Zhang, Y. Zhang, Y. Deng, J. Guan, M. Long, Y. Zheng, R. Zhang, H. Wu, Z. Jiang, Homointerface covalent organic framework membranes for efficient desalination, J. Mater. Chem. 9 (40) (2021) 23178–23187, https://doi.org/10.1039/d1ta06439h.

[21] Y. Fu, S. Su, N. Zhang, Y. Wang, X. Guo, J. Xue, Dehydration-determined ion selectivity of graphene subnanopores, ACS Appl. Mater. Interfaces 12 (21) (2020) 24281–24288, https://doi.org/10.1021/acsami.0c03932.

[22] X. Wang, J. Lu, S. Lu, B. Li, L. Zhang, C. Ma, K. Ma, L. Lin, X. Jiang, B. Yang, Health monitoring of repaired composite structure using MXene sensor, Compos. Commun. 27 (2021), 100850, https://doi.org/10.1016/j.coco.2021.100850.

[23] F. Liao, Z. Xu, Z. Fan, Q. Meng, B. Lv, X. Ye, C. Shen, G. Zhang, Confined assembly of ultrathin dual-functionalized Z-MXene nanosheet intercalated GO nanofilms with controlled structure for size-selective permeation, J. Mater. Chem. 9 (20) (2021) 12236–12243, https://doi.org/10.1039/d1ta01514a.

[24] J. Wang, Z. Zhang, J. Zhu, M. Tian, S. Zheng, F. Wang, X. Wang, L. Wang, Ion sieving by a two-dimensional Ti_3C_2Tx alginate lamellar membrane with stable interlayer spacing, Nat. Commun. 11 (1) (2020) 3540, https://doi.org/10.1038/s41467-020-17373-4.

[25] Z. Du, K. Chen, Y. Zhang, Y. Wang, P. He, H. Mi, Y. Wang, C. Liu, C. Shen, Engineering multilayered MXene/electrospun poly(lactic acid) membrane with increscent electromagnetic interference (EMI) shielding for integrated joule heating and energy generating, Compos. Commun. 26 (2021), 100770, https://doi.org/10.1016/j.coco.2021.100770.

[26] L. Guo, Y. Yang, F. Xu, Q. Lan, M. Wei, Y. Wang, Design of gradient nanopores in phenolics for ultrafast water permeation, Chem. Sci. 10 (7) (2019) 2093–2100, https://doi.org/10.1039/c8sc03012j.

[27] J. Zhu, L. Wang, J. Wang, F. Wang, M. Tian, S. Zheng, N. Shao, L. Wang, M. He, Precisely tunable ion sieving with an Al_{13}-$Ti_3C_2T_x$ lamellar membrane by controlling interlayer spacing, ACS Nano 14 (11) (2020) 15306–15316, https://doi.org/10.1021/acsnano.0c05649.

[28] L. Ding, Y. Wei, Y. Wang, H. Chen, J. Caro, H. Wang, A two-dimensional lamellar membrane: MXene nanosheet stacks, Angew. Chem. Int. Ed. 56 (7) (2017) 1825–1829, https://doi.org/10.1002/anie.201609306.

[29] Q. Long, S. Zhao, J. Chen, Z. Zhang, G. Qi, Z. Liu, Self-assembly enabled nano-intercalation for stable high-performance MXene membranes, J. Membr. Sci. 635 (2021), 119464, https://doi.org/10.1016/j.memsci.2021.119464.

[30] X. Sui, Y. Wang, F. Liu, Z. Yuan, C. Wang, Y. Yu, K. Zhou, K. Goh, Y. Chen, The tripartite role of 2D covalent organic frameworks in graphene-based organic solvent nanofiltration membranes, Matter 4 (9) (2021) 2953–2969, https://doi.org/10.1016/j.matt.2021.06.043.

[31] Q. Lan, C. Feng, Z. Wang, L. Li, Y. Wang, T. Liu, Chemically laminating graphene oxide nanosheets with phenolic nanomeshes for robust membranes with fast desalination, Nano Lett. 21 (19) (2021) 8236–8243, https://doi.org/10.1021/acs.nanolett.1c02683.

[32] S. Han, Z. Mai, Z. Wang, X. Zhang, J. Zhu, J. Shen, J. Wang, Y. Wang, Y. Zhang, Covalent organic framework-mediated thin-film composite polyamide membranes toward precise ion sieving, ACS Appl. Mater. Interfaces 14 (2) (2022) 3427–3436, https://doi.org/10.1021/acsami.1c19605.

[33] F. Yang, M. Wu, Y. Wang, S. Ashtiani, H. Jiang, A GO-induced assembly strategy to repair MOF nanosheet-based membrane for efficient H_2/CO_2 separation, ACS Appl. Mater. Interfaces 11 (1) (2019) 990–997, https://doi.org/10.1021/acsami.8b19480.

[34] Y.T. Nam, S.J. Kim, K.M. Kang, W.B. Jung, D.W. Kim, H.T. Jung, Enhanced nanofiltration performance of graphene-based membranes on wrinkled polymer supports, Carbon 148 (2019) 370–377, https://doi.org/10.1016/j.carbon.2019.03.090.

[35] X. Sui, Z. Yuan, C. Liu, L. Wei, M. Xu, F. Liu, A. Montoya, K. Goh, Y. Chen, Graphene oxide laminates intercalated with 2D covalent-organic frameworks as a robust nanofiltration membrane, J. Mater. Chem. 8 (19) (2020) 9713–9725, https://doi.org/10.1039/d0ta01727b.

[36] M. Ding, H. Xu, W. Chen, G. Yang, Q. Kong, D. Ng, T. Lin, Z. Xie, 2D laminar maleic acid-crosslinked MXene membrane with tunable nanochannels for efficient and stable pervaporation desalination, J. Membr. Sci. 600 (2020), 117871, https://doi.org/10.1016/j.memsci.2020.117871.

[37] X. Wu, M. Ding, H. Xu, W. Yang, K. Zhang, H. Tian, H. Wang, Z. Xie, Scalable $Ti_3C_2T_x$ MXene interlayered forward osmosis membranes for enhanced water purification and organic solvent recovery, ACS Nano 14 (7) (2020) 9125–9135, https://doi.org/10.1021/acsnano.0c04471.

[38] S. Karan, Z. Jiang, A.G. Livingston, Sub-10 nm polyamide nanofilms with ultrafast solvent transport for molecular separation, Science 348 (6241) (2015) 1347–1351, https://doi.org/10.1126/science.aaa5058.

[39] M. Ding, H. Xu, W. Chen, Q. Kong, T. Lin, H. Tao, K. Zhang, Q. Liu, K. Zhang, Z. Xie, Construction of a hierarchical carbon nanotube/MXene membrane with distinct fusiform channels for efficient molecular separation, J. Mater. Chem. 8 (43) (2020) 22666–22673, https://doi.org/10.1039/d0ta07354g.

[40] X. Li, J. Yang, W. Yuan, P. Ji, Z. Xu, S. Shi, X. Han, W. Niu, F. Yin, Microstructured MXene/polyurethane fibrous membrane for highly sensitive strain sensing with ultra-wide and tunable sensing range, Compos. Commun. 23 (2021), 100586, https://doi.org/10.1016/j.coco.2020.100586.

[41] X. Shi, A. Xiao, C. Zhang, Y. Wang, Growing covalent organic frameworks on porous substrates for molecule-sieving membranes with pores tunable from ultra- to nanofiltration, J. Membr. Sci. 576 (2019) 116–122, https://doi.org/10.1016/j.memsci.2019.01.034.

[42] X. Shi, D. Ma, F. Xu, Z. Zhang, Y. Wang, Table-salt enabled interface-confined synthesis of covalent organic framework (COF) nanosheets, Chem. Sci. 11 (4) (2020) 989–996, https://doi.org/10.1039/c9sc05082e.

[43] Z. Xia, Y. Zhao, Y. Zhao, Covalent organic frameworks for water treatment, Adv. Mater. Interfac. 8 (1) (2021), 2001507, https://doi.org/10.1002/admi.202001507.

[44] B. Gole, V. Stepanenko, S. Rager, M. Gruene, D.D. Medina, T. Bein, F. Wuerthner, F. Beuerle, Microtubular self-assembly of covalent organic frameworks, Angew. Chem. Int. Ed. 57 (3) (2018) 846–850, https://doi.org/10.1002/anie.201708526.

[45] N.A.A. Zwaneveld, R. Pawlak, M. Abel, D. Catalin, D. Gigmes, D. Bertin, L. Porte, Organized formation of 2D extended covalent organic frameworks at surfaces, J. Am. Chem. Soc. 130 (21) (2008) 6678–6679, https://doi.org/10.1021/ja800906f.

[46] Y. Su, X. Yan, Y. Chen, X. Guo, X. Chen, W. Lang, Facile fabrication of COF-LZU1/PES composite membrane via interfacial polymerization on microfiltration substrate for dye/salt separation, J. Membr. Sci. 618 (2021), 118706, https://doi.org/10.1016/j.memsci.2020.118706.

[47] R. Wang, X. Shi, A. Xiao, W. Zhou, Y. Wang, Interfacial polymerization of covalent organic frameworks (COFs) on polymeric substrates for molecular separations, J. Membr. Sci. 566 (2018) 197–204, https://doi.org/10.1016/j.memsci.2018.08.044.

[48] R.P. Pandey, P.A. Rasheed, T. Gomez, R.S. Azam, K.A. Mahmoud, A fouling-resistant mixed-matrix nanofiltration membrane based on covalently cross-linked $Ti_3C_2T_X$ (MXene)/cellulose acetate, J. Membr. Sci. 607 (2020), 118139, https://doi.org/10.1016/j.memsci.2020.118139.

[49] X. Feng, Z. Yu, R. Long, Y. Sun, M. Wang, X. Li, G. Zeng, Polydopamine intimate contacted two-dimensional/two-dimensional ultrathin nylon basement membrane supported RGO/PDA/MXene composite material for oil-water separation and dye removal, Separ. Purif. Technol. 247 (2020), 116945, https://doi.org/10.1016/j.seppur.2020.116945.